Fingerprints of Inelastic Transport at the Surface of the Topological Insulator Bi_2Se_3: Role of Electron-Phonon Coupling

M. V. Costache,[1,*] I. Neumann,[1,2] J. F. Sierra,[1] V. Marinova,[3] M. M. Gospodinov,[4] S. Roche,[1,5] and S. O. Valenzuela[1,2,5,†]
[1]ICN2—Institut Catala de Nanociencia i Nanotecnologia, Campus UAB, Bellaterra, 08193 Barcelona, Spain
[2]Universitat Autònoma de Barcelona, Bellaterra, 08193 Barcelona, Spain
[3]Institute of Optical Materials and Technologies, Bulgarian Academy of Science, Sofia 1113, Bulgaria
[4]Institute of Solid State Physics, Bulgarian Academy of Sciences, 72 Tzarigradsko Chaussee boulevard, 1784 Sofia, Bulgaria
[5]ICREA—Institució Catalana de Recerca i Estudis Avançats, 08010 Barcelona, Spain
(Received 7 August 2013; revised manuscript received 14 November 2013; published 25 February 2014)

We report on electric-field and temperature-dependent transport measurements in exfoliated thin crystals of the Bi_2Se_3 topological insulator. At low temperatures (< 50 K) and when the chemical potential lies inside the bulk gap, the crystal resistivity is strongly temperature dependent, reflecting inelastic scattering due to the thermal activation of optical phonons. A linear increase of the current with voltage is obtained up to a threshold value at which current saturation takes place. We show that the activated behavior, the voltage threshold, and the saturation current can all be quantitatively explained by considering a single optical-phonon mode with energy $\hbar\Omega \approx 8$ meV. This phonon mode strongly interacts with the surface states of the material and represents the dominant source of scattering at the surface at high electric fields.

DOI: 10.1103/PhysRevLett.112.086601 PACS numbers: 72.10.Di, 72.20.Ht, 73.20.-r, 73.25.+i

The observation of surface states protected by time inversion invariance in the Bi_2Se_3 family of materials [1–6] has triggered intense research because of the possibility of developing topological insulator devices at room temperature. However, the properties limiting charge transport, which is key for electronic applications, are still not known in detail. Elastic scattering by disorder imposes a limit to the conductivity of the surface states at low temperatures; nevertheless, as disorder is reduced, the limit at finite temperatures will be ultimately set by the intrinsic electron-phonon (e-ph) coupling. In recent theoretical work a strong e-ph coupling in Bi_2Te_3 was obtained [7,8]. The results are in agreement with temperature-dependent angle-resolved photoemission spectroscopy (ARPES) measurements in Bi_2Se_3 [9,10]. ARPES studies target the electronic structure and integrate the e-ph interaction over all phonon modes. The main dispersive surface optical-phonon branch with an energy $\hbar\Omega$ of about 6–8 meV at the $\bar{\Gamma}$ point was identified by using helium-beam surface scattering, which also showed the absence of Rayleigh phonons [11]. The e-ph coupling constant $\lambda = 0.43$ for this branch was found to be larger than any of the integrated values that are reported with ARPES [12]. Such results are further supported by magneto-optical [13] and Fourier-transform interferometry [14] which found an optical-phonon mode at $\hbar\Omega = 7.6$ meV.

Experimental investigations therefore suggest an anomalously large e-ph coupling for a specific surface-phonon branch, which could be readily observable in electrical transport measurements [15], in particular, because surface states in Bi_2Se_3 carry a large fraction of the current flowing in thin crystals [16–20] and films [21,22]. Additionally, the calculated bulk phonon dispersion curves projected into the surface Brillouin zone also show an optical phonon in the same energy range [11]. However, no fingerprint of an optical-phonon mode on inelastic transport has been reported to date.

In this Letter, by performing temperature- and voltage-dependent transport measurements in Bi_2Se_3 thin crystals, a strong electron-phonon mediated inelastic backscattering phenomenon is unveiled. For temperatures $T < \hbar\Omega/k_B \approx 90$ K (k_B is the Boltzmann constant), the resistance is highly nonlinear and is consistent with a thermally activated behavior dictated by an optical phonon with $\hbar\Omega \simeq 8$ meV , as identified in spectroscopic experiments [11–14]. Moreover, the onset of suppression of the conductance for $eV \gtrsim 10$ meV , in conjunction with current saturation as reported in graphene [23–25], further confirms the influence of a $\hbar\Omega \simeq 8$ meV mode.

The devices were fabricated with single crystals mechanically exfoliated onto a highly doped Si substrate with 280 or 440 nm of thermally grown SiO_2, followed by e-beam lithography, metal deposition, and lift-off. The inset in Fig. 1(c) shows an optical microscope image of a typical device used in the present study. The chosen crystals have an elongated shape to obtain a homogeneous current flow. The distances between the inner and outer electrodes are about 0.3–1 and 2–3 μm, respectively. Four-probe transport measurements down to 4.2 K were performed on six different devices in vacuum, yielding similar results (Table SI [26]). Here we present representative data for two of them with thickness $t = 20$ nm (device $D1$) and $t = 30$ nm (device $D2$).

Figures 1(a) and (b) show the square resistance R as a function of gate voltage V_g for devices $D1$ and $D2$,

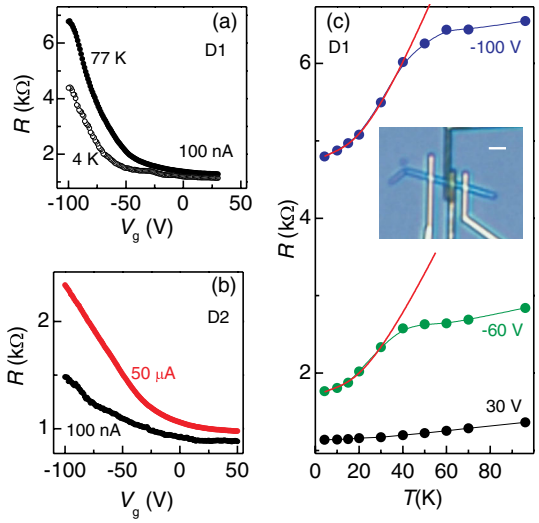

FIG. 1 (color online). (a) Resistance R as a function of the gate voltage V_g at $T = 77$ K (solid symbols) and at $T = 4.2$ K (empty symbols), with applied current $I = 100$ nA, for device $D1$. (b) R vs V_g for device $D2$ at $T = 77$ K, $I = 100$ nA (black symbols), and $I = 50$ μA (red symbols). (c) R vs temperature T for device $D1$ at V_g (+30, −60, and −100 V). The red lines are best fits to Eq. (1). The inset shows an optical image of a cleaved crystal contacted with four electrodes.

respectively. When sweeping V_g from positive to negative values, an increase in R is observed, which is due to the n-type doping commonly observed in Bi_2Se_3 crystals. Figure 1(c) shows R versus temperature T for device $D1$ at three gate voltages (+30, −60, and −100 V) and $I = 100$ nA. For $V_g = 30$ V, R is weakly temperature dependent, presumably because the chemical potential μ lies inside the conduction band and disorder scattering is dominant [18]. In contrast, the temperature dependence of R becomes highly nonlinear when μ is shifted towards the material bulk gap, where the surface transport is expected to dominate [17,18]. This is evident for $V_g = -60$ and −100 V and from weak localization measurements [18,21].

When μ lies inside the gap, the conductance $G = 1/R$ splits into surface G^S and bulk G^B contributions: $G = G^S + G^B$, where G^B results from carrier excitation to the conduction or valence bands, which is more significant for $T \gtrsim 100$ K [18,27]. Hence, the strong temperature dependence for negative V_g at $T < 50$ K suggests an activated process at the surface mediated by inelastic scattering involving a single or multiple phonon modes. Our data can be indeed fitted [red lines in Fig. 1(c)] with an equation that includes only a single Bose-Einstein term, thus a single phonon mode, as follows:

$$R^S(V_g, T) = R_0(V_g) + A(V_g) \times T + B(V_g) \times \left(\frac{1}{e^{\hbar\Omega/k_BT} - 1}\right), \quad (1)$$

where the first term $R_0(V_g)$ accounts for low temperature (residual) resistance due to scattering on static impurities or defects, while the second term is associated to acoustic phonons, for which a linear resistance with temperature has been predicted [7] and recently observed [27].

In Eq. (1), A and B are fitting parameters, where A is independent on V_g for carriers with a linear dispersion relation, that is, for Dirac fermions at the surface [28]. The best fit gives 7.7 ± 1 meV , which corresponds to the energy of the dominant surface phonon branch observed by helium-beam surface scattering [12] and optical methods [13,14]. It could also be due to scattering off bulk optical phonons projected into the surface [11]. The fit, however, is not enough proof to demonstrate that the main scattering mechanism originates from an optical-phonon branch. A power-law dependence expected in some cases for acoustic phonons scattering can also fit the results, and therefore further experiments are necessary [26].

An activated response similar to that in Fig. 1(c) was found in graphene on a SiO_2 substrate [28]. It was argued to originate from remote interfacial phonon scattering by surface optical-phonon modes in SiO_2. Because the lowest energy of the relevant modes exceeds 50 meV, much larger than that in Bi_2Se_3, the activated behavior was observed only at $T > 200$ K. Additionally, the same nonlinear T dependence of R was noted in Ca-doped Bi_2Se_3 crystals, and its onset with V_g was interpreted as μ reaching the lower edge of the conduction band [18]; however, the activated nature of the effect was not discussed [26].

Electrical transport experiments in graphene have shown that the current tends to saturate as the bias voltage is increased above ~200 meV [23–25]. The saturation has been attributed to scattering of electrons by optical phonons, either activated at the SiO_2 surface [23,29] or intrinsic to graphene [24]. If the activation energy observed in Fig. 1(c) was due to an optical-phonon mode, the current in Bi_2Se_3 should also tend to saturate with V. Such saturation behavior is expected for scattering of electrons by optical phonons but not for acoustic phonons. Additionally, the saturation current should be weakly temperature dependent.

A first indication of sublinear I-V response is observed in Fig. 1(b), where an increase in R is evident when a large current $I = 50$ μA is applied. The fact that the relative change of R is much larger when μ is shifted towards the bulk gap [18] supports that the main phenomenon is surface related.

Figures 2 and 3 show our main results. Figure 2 displays the I-V characteristics for different gate voltages V_g at 4.2 K. The current at large negative V_g presents a clear tendency for saturation at $V < 50$ mV, with a smaller saturation current I_S for larger absolute values of V_g. This behavior is consistent with optical-phonon scattering and resembles the behavior observed in graphene, where the current saturation becomes gate dependent and decreases when approaching the Dirac point [23,24].

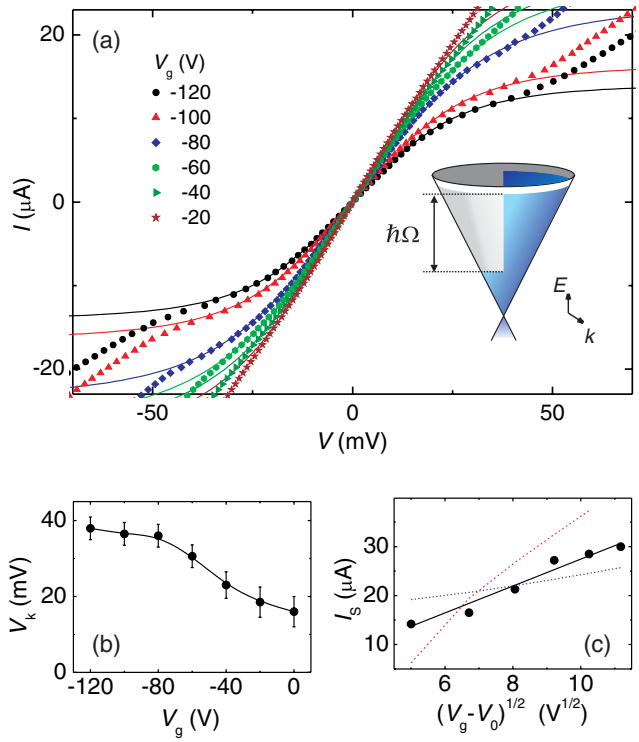

FIG. 2 (color online). (a) Current voltage characteristics I vs V at different V_g (from −20 to −120 V, as labeled) for device $D2$. The lines are best fit to a current saturation model (see the text). (b) Position of the voltage kink V_k as a function of V_g. The line is a guide to the eye. (c) Saturation current I_S vs V_g (black circles). The lines are best fits to Eq. (2) with both V_0 and $\hbar\Omega$ as fitting parameters, resulting in $V_0 = -145$ V and $\hbar\Omega = 8$ meV (solid black). Best fits for fixed $\hbar\Omega = 5$ meV (dotted blue) and $\hbar\Omega = 12$ meV (dotted red) are shown for comparison.

However, $I(V)$ also shows a kink at $V \sim 40$ mV. As discussed below, this feature is likely to be associated to carrier excitations into the conduction and/or valence bands.

Because the saturation is not complete, we approximate I by a saturation model for further analysis. Having compared the fit of our data with different analytical expressions [23,30–32], we found that, as in graphene [32], the best results are obtained by using $I(V) = G_0 V/[1 + (G_0 V/I_S)^{\beta}]^{1/\beta}$, where G_0 is the gate-dependent conductance at low V, and β and the saturation current I_S are fitting parameters. We fitted the data up to the position of the kink V_k, which is determined by the minimum in dI/dV [26]. The gate dependence of $V_k(V_g)$ is shown in Fig. 2(b). The above equation with $\beta = 2.5$ gives the best fit, regardless of the value of V_g [lines in Fig. 2(a)]; the extracted values of I_S are shown in Fig. 2(c).

In order to model I_S, we note that, for instantaneous phonon emission, a steady-state population is established in which right-moving electrons are populated to a higher energy $\hbar\Omega$ than left-moving ones [24,33] [see the inset in Fig. 2(a)]. I_S can then be estimated by integrating the electrons velocity over the steady-state population, which for Dirac fermions and two coupled surfaces results in [24,34]

$$I_S \approx \frac{W}{\pi^{3/2}\hbar}\hbar\Omega\sqrt{eC_g(V_g - V_0)}, \tag{2}$$

where W is the width of the sample and C_g the back gate capacitance. V_0 is the gate voltage at which μ is tuned at the Dirac point.

Even though we cannot access V_0, because the threshold for breakdown of the SiO_2 dielectric is reached first, direct comparison with results in Ca-doped Bi_2Se_3 crystals [18] together with the incipient rounding of the $R(V_g)$ response [Figs. 1(b) and 1(c)] suggests that V_0 is within a few tens of volts beyond the breakdown. Indeed, Eq. (2) gives a good fit to I_S vs V_g with $V_0 \approx -145$ V [Fig. 2(c)]. From the fit, we obtain $\hbar\Omega = 8.1 \pm 1.5$ meV , which is in remarkable agreement with the activation energy estimated from the data in Fig. 1. Additionally, Fig. 2(c) shows the large discrepancy between the experimental data and the theoretical I_S by using Eq. (2) for $\hbar\Omega$ equal to 5 and 12 meV, which further yield unrealistic values of V_0 (−245 and −120 V, respectively). This demonstrates that $\hbar\Omega$ must be in a very restricted range of energies.

Figure 3 shows the conductance $G(V)$ at specific gate voltages. At high positive V_g, G presents a smooth decrease with V, which is typical of a bulk metal in which the dominant scattering mechanism is disorder. At large negative V_g, when activation effects in Fig. 1 become evident, G develops a plateaulike feature under the action of a weak electric field. There, the only contribution to the resistance comes from elastic scattering induced by static disorder. The increase of the bias voltage leads to an energy gain by the propagating electrons, which eventually reaches the energy threshold that allows for an electron-phonon scattering event (such as phonon emission). A new inelastic

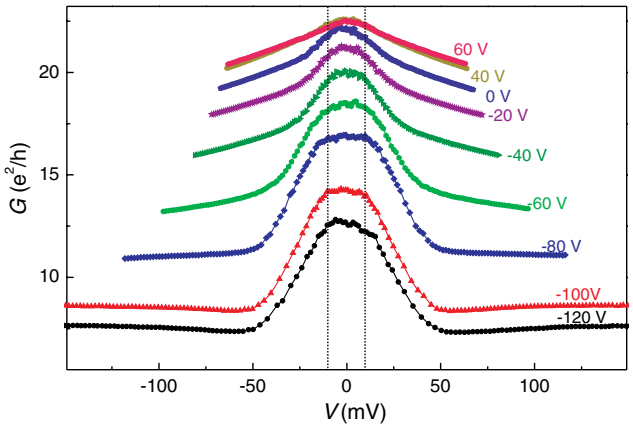

FIG. 3 (color online). Conductance ($G = I/V$) vs V at fixed gate voltages V_g (from −120 to +60 V) and at $T = 4.2$ K for device $D2$.

transport length scale then enters into play and brings about an additional contribution to the resistance, which adds up to the elastic one, in virtue of the Matthiessen rule. At fixed gate voltage (or Fermi level position), the elastic part is given by the measured resistance at low temperature and zero bias, whereas the inelastic contribution is bias dependent. The onset for phonon scattering occurs at about 10 mV (pinpointed by vertical lines in Figs. 3 and 4), while in this crystal the suppression of the conductance becomes significant only beyond 20–30 mV.

We now focus on the origin of the kink in the I-V characteristics [Fig. 2(a)]. The position of the kink V_k, which is given in Fig. 2(b), is weakly dependent on V_g for $V_g < -80$ V but drops quickly as V_g approaches zero, becoming undetectable for positive V_g, which coincides with $eV_k \sim \hbar\Omega$.

The kink can be due to excitations of carriers into the conduction and/or valence bands [15,18,27]. A similar gate-driven transformation to a conductor with strong temperature dependence [Fig. 1(c)] was reported in Ref. [18] and associated to the opening of an effective bulk gap $\Delta \sim 50$ meV that results from gap narrowing due to band bending (the intrinsic bulk gap in Bi_2Se_3 is about 300 meV). At low temperatures, the presence of such a gap is essential for observing signatures of surface states. However, at high enough temperatures, thermal excitation of carriers from remnant electron pockets to the conduction band can enhance the bulk transport contribution [18,26]. The transfer of electrons from the electron pockets to the conduction band can also be driven by high electric fields, which for $V = 50$ meV exceed 1 kV/cm. Such transitions are known to occur in GaAs between conduction valleys [31]. This explanation is further supported by the increase of V_k as the chemical potential is moved deeper into the gap; however, the weak dependence for $V_g < -80$ V remains unexplained. Thermal activation of a bulk channel was also observed in Ref. [27] but ascribed to the activation of electrons from the bulk valence band to the surface band. It is plausible that the overall response of V_k results from the combination of these two phenomena, and thus $V_g \sim -80$ V may signal the onset of electron transfer from the valence band that prevents V_k from further increasing.

Figure 4 displays $G(V)$ at $V_g = -100$ V for T between 4.2 and 70 K. G is strongly temperature dependent for $|V| < 50$ mV. Over this V range and for $T < 40$ K, G presents the same activated behavior that is observed at low V, with a characteristic energy of about 8 meV (inset). In contrast, G is largely temperature independent for $V > 50$ mV. This is typical of a disordered metal, a behavior that was found when μ lies in the bulk conduction band [Fig. 1(c)], which is in agreement with the hypothesis of electron transfer into bulk channels. Finally, the observation of I_S being nearly independent of T despite significant change in G further supports the origin of the saturation as being related to a single optical-phonon branch [26].

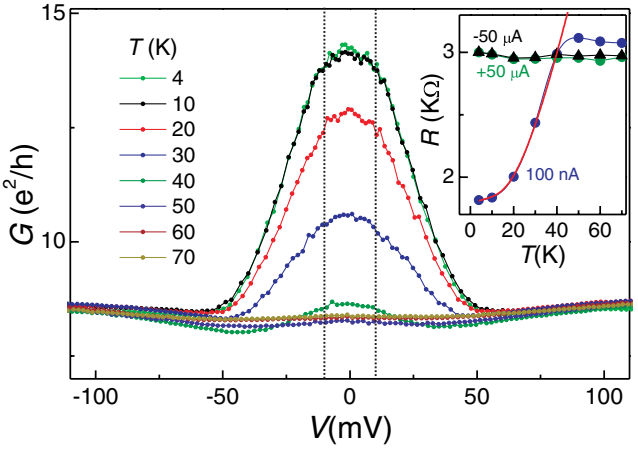

FIG. 4 (color online). G vs V at fixed T (from 4 to 70 K) for $V_g = -100$ V. Inset: R vs T inferred from data shown in the main panel at $I = 100$ nA, $+50$ μA, and -50 μA. The red line is the best fit to Eq. (1).

In conclusion, our results show compelling evidence of a strong e-ph coupling involving an optical-phonon mode with $\hbar\Omega \approx 8$ meV that mediates inelastic scattering. The thermally activated behavior of the Bi_2Se_3 resistance at low temperatures, the voltage at which inelastic scattering emerges, and the magnitude of the saturation current at high voltage and its independence of temperature are all consistent with this interpretation. This is reinforced by helium scattering experiments, which identified a main phonon mode at 6–8 meV and the absence of acoustic Rayleigh phonons [11,12], and theoretical calculations that show a bulk optical phonon that projects into the surface Brillouin zone in the same energy range [11]. The transport experiments carried out here are in a less controlled environment than those in Refs. [11,12]. However, the surface states in Bi_2Se_3 have proven to be robust to processing, and, in particular, the relevant surface phonon mode was observed even after exposure to air [13].

We acknowledge the support from the European Research Council (ERC Grant Agreement No. 308023 SPINBOUND), MINECO (MAT2010-18065, MAT2012-33911, and RYC-2011-08319), and AGAUR (Beatriu de Pinós program).

*mcostache@icn.cat
†SOV@icrea.cat

[1] M. Z. Hasan and C. L. Kane, Rev. Mod. Phys. **82**, 3045 (2010).
[2] X.-L. Qi and S.-C. Zhang, Rev. Mod. Phys. **83**, 1057 (2011).
[3] J. E. Moore, Nature (London) **464**, 194 (2010).

[4] C. Brüne, C. X. Liu, E. G. Novik, E. M. Hankiewicz, H. Buhmann, Y. L. Chen, X. L. Qi, Z. X. Shen, S. C. Zhang, and L. W. Molenkamp, Phys. Rev. Lett. **106**, 126803 (2011).
[5] Y. Xia, D. Qian, D. Hsieh, L. Wray, A. Pal, H. Lin, A. Bansil, D. Grauer, Y. S. Hor, R. J. Cava, and M. Z. Hasan, Nat. Phys. **5**, 398 (2009).
[6] H. J. Zhang, C. X. Liu, X. L. Qi, X. Dai, Z. Fang, and S. C. Zhang, Nat. Phys. **5**, 438 (2009).
[7] S. Giraud and R. Egger, Phys. Rev. B **83**, 245322 (2011).
[8] S. Giraud, A. Kundu, and R. Egger, Phys. Rev. B **85**, 035441 (2012).
[9] R. C. Hatch, M. Bianchi, D. Guan, S. Bao, J. Mi, B. B. Iversen, L. Nilsson, L. Hornekaer, and P. Hofmann, Phys. Rev. B **83**, 241303 (2011).
[10] C. Chen *et al.*, Sci. Rep. **3**, 2411 (2013).
[11] X. Zhu, L. Santos, R. Sankar, S. Chikara, C. Howard, F. C. Chou, C. Chamon, and M. El-Batanouny, Phys. Rev. Lett. **107**, 186102 (2011).
[12] X. Zhu, L. Santos, C. Howard, R. Sankar, F. C. Chou, C. Chamon, and M. El-Batanouny, Phys. Rev. Lett. **108**, 185501 (2012).
[13] A. D. LaForge, A. Frenzel, B. C. Pursley, T. Lin, X. Liu, J. Shi, and D. N. Basov, Phys. Rev. B **81**, 125120 (2010).
[14] P. Di Pietro *et al.*, Nat. Nanotechnol. (to be published).
[15] P. Zhang and M. W. Wu, Phys. Rev. B **87**, 085319 (2013).
[16] H. Peng *et al.*, Nat. Mater. **9**, 225 (2010).
[17] H. Steinberg, D. R. Gardner, Y. S. Lee, and P. Jarillo-Herrero, Nano Lett. **10**, 5032 (2010).
[18] J. G. Checkelsky, Y. S. Hor, R. J. Cava, and N. P. Ong, Phys. Rev. Lett. **106**, 196801 (2011).
[19] B. Sacepe, J. B. Oostinga, J. Li, A. Ubaldini, N. J. G. Couto, E. Giannini, and A. F. Morpurgo, Nat. Commun. **2**, 575 (2011).
[20] F. Xiu *et al.*, Nat. Nanotechnol. **6**, 216 (2011).
[21] H. Steinberg, J.-B. Laloe, V. Fatemi, J. S. Moodera, and P. Jarillo-Herrero, Phys. Rev. B **84**, 233101 (2011).
[22] A. Kandala, A. Richardella, D. Zhang, T. C. Flanagan, and N. Samarth, Nano Lett. **13**, 2471 (2013).
[23] I. Meric, M. Y. Han, A. F. Young, B. Özyilmaz, P. Kim, and K. L. Shepard, Nat. Nanotechnol. **3**, 654 (2008).
[24] A. Barreiro, M. Lazzeri, J. Moser, F. Mauri, and A. Bachtold, Phys. Rev. Lett. **103**, 076601 (2009).
[25] L. E. F. Foa Torres and S. Roche, Phys. Rev. Lett. **97**, 076804 (2006).
[26] See Supplemental Material at http://link.aps.org/supplemental/10.1103/PhysRevLett.112.086601 for more experimental data and discussion.
[27] D. Kim, Q. Li, P. Syers, N. P. Butch, J. Paglione, S. Das Sarma, and M. S. Fuhrer, Phys. Rev. Lett. **109**, 166801 (2012).
[28] J. H. Chen, C. Jang, S. Xiao, M. Ishigami, and M. S. Fuhrer, Nat. Nanotechnol. **3**, 206 (2008).
[29] B. Scharf, V. Perebeinos, J. Fabian, and I. Žutić, Phys. Rev. B **88**, 125429 (2013).
[30] C. Canali, G. Majni, R. Minder, and G. Ottavianni, IEEE Trans. Electron Devices **22**, 1045 (1975).
[31] S. M. Sze, *Semiconductor Devices* (Wiley, New York, 1985).
[32] V. E. Dorgan, M.-H. Bae, and E. Pop, Appl. Phys. Lett. **97**, 082112 (2010).
[33] Z. Yao, C. L. Kane, and C. Dekker, Phys. Rev. Lett. **84**, 2941 (2000).
[34] In deriving Eq. (2), we considered the second expression of Eq. (1) from Ref. [24]; due to the low energy of the relevant phonon modes, we assumed $(\hbar\Omega)^2/4 \ll [C_g V_g (\hbar v_F)^2 \pi]/e$, a condition that is later verified by the fitting results.